Journal of
Ceramic Science
and Technology

J. Ceram. Sci. Tech., **05** [02] 145-154 (2014)
DOI: 10.4416/JCST2013-00041
available online at: http://www.ceramic-science.com

Numerical Prediction of Effective Thermal Conductivity of Refractory Materials: Methodology and Sensitivity Analysis

R. Zehmisch[1], C. Demuth[*1], A. Al-Zoubi[1], M.A.A. Mendes[1], F. Ballani[2], S. Ray[1], D. Trimis[1]

[1]Institute of Thermal Engineering, Technische Universität Bergakademie Freiberg, Gustav-Zeuner-Straße 7, D-09596 Freiberg, Germany
[2]Institute of Stochastics, Technische Universität Bergakademie Freiberg, Prüferstraße 9, D-09596 Freiberg, Germany

received November 10, 2013; received in revised form January 20, 2014; accepted March 14, 2014

Abstract

The present paper deals with numerical predictions of the effective thermal conductivity (k_{eff}) of refractory materials. The composite is modelled using a geometry generation method; either the Coloured Dead Leaves Model (CDLM) or the modified version of the Random Sequential Adsorption (RSA) algorithm, for coarse grain components. On the other hand, there are constituents which could not be resolved by the computational model and are, therefore, treated as a continuous interstitial phase, termed as the 'unresolved' or the 'rest' material. The generated random geometry is discretised employing a uniform grid in the computational domain, where the heat conduction equation is solved with either the Thermal Lattice-Boltzmann Method (TLBM) or the Finite Volume Method (FVM). From the steady-state solution of the heat conduction equation, k_{eff} is determined using a simple averaged relation. This investigation also comprises the sensitivity analysis of the presented methodology with regard to the isotropy of generated geometry, the reproducibility of results, the employed shape of grains and the unknown thermal conductivity of 'rest' material. Results indicate that k_{eff} is linearly dependent on the last, whereas it is nearly insensitive to other parameters.

Keywords: Effective thermal conductivity, refractory materials, thermal lattice-Boltzmann method, random sequential adsorption, sensitivity analysis

I. Introduction

Refractory materials are of vital importance in high-temperature processes encountered in the steel, cement, petrochemical industries, processes involving energy conversion, etc. [1] Research is being conducted continuously in order to improve the quality and energy efficiency of these processes, while focussing on a significant reduction of CO_2 emissions. Therefore, new refractory materials are developed where the carbon content is reduced with an aim to make them as free of carbon as possible. At the same time, the involved refractories should be resistant against thermal shock and corrosion and should have good thermal insulation properties.

The materials of present interest are oxidic ceramics with additives; to be more precise, carbon-bonded alumina refractories. These composite materials exhibit a complex porous microstructure with fibroid and/or granular additional components embedded within the matrix. The type and shape of additional components are expected to affect the resulting properties of the refractory. For the application of refractory materials, their thermal properties, particularly the effective thermal conductivity (k_{eff}), are of utmost significance. With a reduction of the carbon content, k_{eff} of the refractory material is also reduced. Owing mainly to this reason, the prediction of k_{eff} of such complex materials is essential. The effective thermal conductivity, however, can be determined either experimentally or numerically.

Thermal conductivity of carbon-containing refractories was determined from experiments using hot-wire method at temperatures up to 800 °C by Tomeczek and Suwak [2]. On the other hand, Barea *et al.* [3] employed the laser flash method in order to measure the thermal diffusivity a of Al_2O_3/SiC platelet composites, from room temperature up to 1000 °C, as a function of SiC platelet content varying from 0 to 30 vol% and calculated thermal conductivities of composites from thermal diffusivities using the tabulated density ϱ and specific heat c_p data of the components.

Numerical determination of k_{eff} of complex materials was performed by numerous authors using a variety of methods. Veyret *et al.* [4] employed a Finite Element (FE) formulation in order to numerically determine k_{eff} of diphasic composites. Effective thermal conductivity of polymer-matrix composites with high filler loading was determined by Zhou *et al.* [5], who proposed a model of heat transfer passages and compared the results with a Finite Difference (FD) formulation solving Laplace equation in a Representative Volume Element (RVE) and with

* Corresponding author: cornelius.demuth@iwtt.tu-freiberg.de

Maxwell's model [6] of k_{eff} for composites. The Finite Volume Method (FVM) was employed by Petrasch *et al.* [7] in order to determine the effective thermal conductivity of reticulate porous ceramics. The effective thermal conductivity of functionally graded materials with random heterogeneous microstructure was predicted by Dondero *et al.* [8] using RVEs and a modified Boundary Element Method (BEM).

In the past decade, however, determination of effective thermal conductivity employing the Thermal Lattice-Boltzmann Method (TLBM) [9], where macroscopic energy conservation is represented by the Lattice-Boltzmann Equation (LBE) [9], became popular due to the ease of implementation of interparticle interaction and boundary conditions on complex geometries [9,10]. Furthermore, as will be shortly apparent, owing to the local nature of TLBM formulation, the implementation is also extremely easy to parallelise. Wang and Pan [10] reviewed the determination of effective properties, particularly employing LBM. Qian *et al.* [11] calculated k_{eff} of porous media by means of a two-dimensional (2D) lattice-Boltzmann model. The prediction of k_{eff} using TLBM was demonstrated by Wang *et al.* for 2D [12] and 3D [13] random porous media. Wang and his co-workers also applied TLBM in order to determine k_{eff} of several other types of materials, e.g. 2D random natural fibrous materials [14], 2D multiphase microgranular porous media [15], 3D functionally graded materials [16], etc.

Complex composite refractory materials can be numerically modelled using stochastic geometry generation algorithms. For this reason, special attention is required in order to be able to neglect effects of anisotropy and randomness of the generated multiphase computational domain. In addition, the combined thermal conductivity of components, those cannot be resolved by the modelled geometry, is likely to influence k_{eff} of the modelled material. The major objective of this article, therefore, is to carry out a systematic sensitivity analysis of the predicted effective thermal conductivity using the TLBM as well as the FVM.

The present article is divided into five sections. After this introduction, details of preparation of considered materials and experimentally determined properties relevant for modelling refractories are outlined in the experimental section. In the third section, the numerical methodology consisting of stochastic geometry generation and numerical solution of heat conduction equation by either TLBM or FVM is explained. The following section presents results obtained from the sensitivity analysis along with their discussion. Finally, conclusions are drawn and an outlook on the prospective study is presented in section V.

II. Experimental

Novel Al_2O_3-C refractory materials were developed at the Institute of Ceramics, Glass and Construction Materials of Technische Universität Bergakademie Freiberg. The weight fractions of the constituents of considered compositions are given in Table 1 [17–19]. Including nanoscaled additives [17–19] in the composition allows for a reduction of carbon content in the refractory material, while maintaining or even enhancing thermomechanical properties [19]. In this attempt, specifically magnesium aluminate spinel ($MgAl_2O_4$), alumina sheets (α-Al_2O_3) and multi-wall carbon nanotubes (CNTs) were added as nanoscaled particles [17–19]. Considered materials are named S10, where 0.1 wt% of magnesium aluminate spinel is added to the weight fractions of Reference 3 composition in Table 1, AS and BT. Latter materials are characterised by the composition of Reference 2 in Table 1 with an additional 0.1 wt% of alumina sheets in AS and 0.5 wt% of multi-wall carbon nanotubes for BT.

Table 1: Weight fractions of raw materials before coking for three reference compositions of the refractory [17–19].

Raw materials	Compositions (wt%)		
	Reference 1	Reference 2	Reference 3
Fused alumina	25.3	29.1	33.4
Tabular alumina	33.7	38.9	44.6
Fine graphite	14.5	10.0	5.0
Coarse graphite	14.5	10.0	5.0
Novolac liquid	2.0	2.0	2.0
Novolac powder	4.0	4.0	4.0
Silicon	6.0	6.0	6.0
Sum	100.0	100.0	100.0
Hexamethylene-tetramine	0.6	0.6	0.6

Present composite ceramic materials were produced in a batch process. The individual components were consecutively weighed in a large bowl using electronic scales and subsequently added to an Eirich mixer according to the weight composition. The overall mass of the complete mixture before coking was in the range of 6000 – 7000 g. An error of the order 1 g, due to the inaccuracy in manually adding the exact mass fraction and limited accuracy of scales, could be reasonably assumed for each component. In terms of the stated overall mass, this means that the mass fraction of each individual constituent is accurate to 0.02 wt%. In detail, mass fractions of components greater than or equal to 5 wt% of main constituents, i.e. alumina, graphite and silicon grains, are accurate to 0.1 – 0.3 %, while lower mass fractions of binder constituents and curing agent are accurate to 1 – 3 %. In addition, low weight fractions of nanoscaled additives with less than or equal to 0.5 wt% are accurate to 3 – 15 %. However, particular attention should be paid to the mass fraction of liquid novolac that had to be poured in a separate small vessel before adding to the mixture and the addition of exact mass fraction of this gluey high-viscosity liquid was even more difficult. Therefore, allowing for an error of 2 g in the liquid novolac content, its weight fraction can be considered to be accurate to 2 %.

Selected raw materials were mixed in the Eirich intensive mixer at room temperature and thereafter samples were uniaxially pressed at 100 MPa. The pressed samples were cured at 180 °C and subsequently coked under re-

ducing environment at either 1000 °C or 1400 °C for 5 h. The open porosity, bulk density and pore size distribution were determined using a mercury porosimeter. Further details are provided by Roungos *et al.* [17] and Roungos and Aneziris [18].

In order to model the refractory material, volume fractions of its components after the coking process have to be estimated. Therefore, the residual carbon content, i.e. the mass fraction of carbon, remaining after polymerisation of the phenolic resin (novolac) binder with hexamethylenetetramine, with respect to the binder before polymerisation [20], is required. Residual carbon content of novolac is reported in the literature, where values ranging from 45 – 50 % [20,21] up to 60 % for a hexamethylenetetramine content of 10 phr [22] (parts per hundred of resin) can be found.

During the present investigation, the following procedure is applied in order to determine the adopted volume fractions from the mass fractions w_n, reported in Table 1. First, representative volume fractions are determined from the mass fractions as $V_{\mathrm{rep},n} = w_n/\varrho_n$, where ϱ_n is the density of n^{th} material. The overall representative volume is then calculated by $V_{\mathrm{rep}} = \sum_n V_{\mathrm{rep},n}/(1 - p)$, where p is the measured porosity, as given in Table 2. Finally, volume fractions are obtained as $\phi_n = V_{\mathrm{rep},n}/V_{\mathrm{rep}}$. In this calculation, the residual carbon content is assumed to be 45 % and the employed densities of components are $\varrho_{Al_2O_3} = 4\ \mathrm{g/cm^3}$ for all considered types of alumina, $\varrho_{C_{\mathrm{graphite}}} = 2\ \mathrm{g/cm^3}$, $\varrho_{C_{\mathrm{amorphous}}} = 1.8\ \mathrm{g/cm^3}$, [23] $\varrho_{\mathrm{Si}} = 2.33\ \mathrm{g/cm^3}$, [23] $\varrho_{MgAl_2O_4} = 3.6\ \mathrm{g/cm^3}$ [24] and $\varrho_{\mathrm{MWCNT}} = 1.7\ \mathrm{g/cm^3}$ [25,26]. Resulting volume fractions of considered compositions are presented in Table 2 along with thermal conductivities of individual raw materials.

Conceivable deviations of volume fractions of components could be assessed by individually considering ranges of density for each component and determining volume fractions as outlined in the foregoing text. Considered ranges of density are 3.95 – 4.1 g/cm^3 for alumina [24,27], 1.9 – 2.3 g/cm^3 for fine and coarse graphite [23], 1.8 – 2.1 g/cm^3 for amorphous carbon [23], 3.5 – 4.1 g/cm^3 for spinel [24,27] and 1.7 – 1.9 g/cm^3 for multi-wall carbon nanotubes [25,26,28]. For silicon, however, the density is found as $\varrho_{\mathrm{Si}} = 2.33\ \mathrm{g/cm^3}$ [23] and hence no such range could be specified. In addition, the residual carbon content mentioned here is assumed in the range of 45 – 60 %. From these variations of density of individual components, deviations in the resulting volume fractions can be assessed in a straightforward manner.

With respect to Table 2, estimated volume fractions of fused and tabular alumina could be 2 % lower due to higher density or 1 % higher due to lower density. For graphite grains, deviations as compared to the listed values could be observed in the range from -11 % to +4 % for S10 composition and from -10 % to +3 % for AS and BT compositions. The volume fraction of amorphous carbon could be 15 % lower or 30 % higher than those stated in Table 2 due to higher residual carbon content. The volume fraction of magnesium aluminate spinel could be 12 % lower or 3 % higher than the calculated value because of different density. For alumina sheets, the statement given before for other alumina constituents would apply. However, for both spinel and alumina sheets with a mass fraction of only 0.1 wt%, the resulting volume fractions are always rounded up to 0.1 % and, therefore, deviations would not be visible in terms of 0.1 % accuracy of volume fractions given in Table 2. Considering an increased density of multi-wall carbon nanotubes, the resulting volume fraction decreases by 10 % and could be rounded down to 0.4 %.

Table 2: Thermal conductivities of raw materials and their volume fractions in the developed compositions after coking.

Raw materials	Thermal conductivity [W/mK]	Volume fractions [%]		
		S10 comp.	AS comp.	BT comp.
Fused alumina	31.8	24.1	19.7	19.3
Tabular alumina	31.8	32.1	26.3	25.8
Fine graphite	119.0 – 165.0	7.2	13.6	13.3
Coarse graphite	119.0 – 165.0	7.2	13.6	13.3
Amorphous carbon	1.98	4.3	4.1	4.0
Silicon	142.2	7.4	7.0	6.8
Porosity	0.0261	17.6	15.6	17.0
Spinel ($MgAl_2O_4$)	22.0	0.1	–	–
Alumina sheets (α-Al_2O_3)	31.8	–	0.1	–
Carbon nanotubes	300.0	–	–	0.5

For all constituents except silicon, spinel and alumina sheets, the uncertainty in density dominates the estimation of error in volume fraction. However, for silicon, where there is no obvious range of density, and for nanoscaled spinel and alumina sheets with an extremely small mass fraction of 0.1 wt%, the stated error in mass fraction dominates. For these nanoscaled additives, resulting volume fractions still remain unaltered in terms of the accuracy given in Table 2 due to rounding up. The most critical issue, however, is the volume fraction of amorphous carbon, because the cited error in dosing liquid novolac is augmented by uncertainties in both residual carbon content and the density of amorphous carbon.

In order to compare the numerically predicted results, for this study, thermal diffusivities of developed materials were measured at room temperature using the laser flash technique. In addition, specific heats of these materials were determined using the high-temperature calorimeter. With these two measurements and the knowledge of densities of individual materials, the effective thermal conductivity of a given refractory material can be determined as the product of all three quantities. In this manner, the

effective thermal conductivities of compositions S10, AS and BT at room temperature (20 °C) were determined as 37.73 W/mK, 37.06 W/mK and 36.75 W/mK, respectively.

In addition, grain size fractions of individual constituents were determined by the sieve analysis. In this way, a mass distribution over different grain size fractions was obtained. This mass distribution can be converted to a distribution of particle number by considering a representative particle mass for each grain size fraction. The representative particle mass was obtained from the particle volume considering an average particle size in the particular basket as well as the density of considered raw material. Although the mass distribution with respect to the grain size might show certain similarity to a normal distribution, the actual particle number distribution is given by a lognormal distribution [29,30]. This is also true for the refractory materials used for the present study.

Furthermore, the shape of grains of different components was determined by analysing the Scanning Electron Microscopy (SEM) images of developed refractory materials. The shapes of grains identified in this manner for different components are pentagonal polyhedra for fused and tabular alumina grains, hexagonal plates for coarse graphite platelets and spheres for silicon powder.

III. Numerical Methodology

The numerical prediction of the effective thermal conductivity of refractory materials consists of two basic parts. First, the geometry of refractory is modelled using a geometry generation algorithm as described in subsection III.(1). The heat conduction equation with appropriate boundary conditions is then solved for this geometry using the Thermal Lattice-Boltzmann Method (TLBM) and the effective thermal conductivity is determined from the steady-state solution, as further shown in subsection III.(2). In addition, the Finite Volume Method (FVM), described in subsection III.(3), is also employed in order to solve the heat conduction equation for some of the cases, presented in this article.

(1) Geometry generation

Once the actual volume fractions, the approximate grain size distribution functions and the grain shapes of modelled constituents of the refractory material are known, the synthetic geometry of the composite material, to be used subsequently as the computational domain, can be generated. In the present investigation, either a Coloured Dead Leaves Model (CDLM) or a modified Random Sequential Adsorption (RSA) algorithm is employed in order to generate the artificial refractory geometry that mimics the reality as far as possible. For this purpose, first, the grain-sizes (radii) of individual components to be included in the computational domain are randomly generated, according to the lognormal distribution of grain size, with parameters obtained from the results of the sieve analysis.

The original dead leaves model [31] represents a superposition of random closed sets, following which, grains are placed randomly in the computational domain. When the volume fraction of present component is reached, the placement of grains of the next component is taken up. If the position of a new grain overlaps with an already existing grain, the overlapping volume fraction of the new grain is disregarded and only the remaining grain fraction is added to the domain. In this manner, the overall volume fractions of already arranged components are kept unchanged.

In the classical RSA [32,33] algorithm, on the other hand, spheres of random radii are placed sequentially and randomly in a bounded domain [34]. If the placement of a new sphere results in its intersection with an already existing sphere that is successfully placed, the new sphere is rejected and the placement of a next sphere with both a new position and a new radius is attempted [34]. This procedure is stopped when the 'jamming state' is reached, i.e. when it is impossible to place any additional sphere [34].

Since the original RSA algorithm does not allow packing of materials with a high volume fraction, it requires modification in order to meet the present requirement. In the modified RSA algorithm, grains of different components with their specific individual shapes (may be non-spherical) are placed consecutively. For each component, grains are placed until the desired volume fraction is reached. As a modification, grains now representing the same raw material are allowed to overlap with each other, while the placement of a new grain is rejected if it overlaps with the grain of a different material. A typical generated geometry representing the refractory as well as its discretisation on a uniform Cartesian grid is shown in Fig. 1.

With respect to the geometry generation algorithm, it is important to note that in general, the complex shapes of grains are not rotationally symmetric. Therefore, a random rotation by the Euler angles is generated and applied to every grain to be placed. This rotation is performed according to either the so-called 'x-convention' [35] or the international aerospace standard [36]. However, owing to conditions explained before, if a random position of grain placement is rejected, the rotation should not be generated anew for the next attempt, since otherwise anisotropy of the modelled material will result.

A previous study [37], conducted by some of the present authors, showed that the volume represented by the computational model can be specified as a cube of side 2 mm and that reasonable results are obtained using a grid resolution consisting of $200^3 = 8 \times 10^6$ nodes, such that a minimum length of 10 μm could be resolved. As mentioned in the previous section, modelled grains considered in the present study are fused and tabular alumina with the shape of pentagonal polyhedra, coarse graphite in the form of hexagonal polyhedra and silicon grains of spherical shape, all with different respective grain size distributions, obtained from experimental pre-processing. The remaining components, i.e. fine graphite, amorphous carbon and porosity, have the structure of very fine grains beyond the minimum resolution, embedded in a continuous phase (amorphous carbon, in this case), and hence could not be resolved with the present computational model. These components altogether are modelled as the continuous fine-scaled material and may be represented either as the 'rest' material or as the 'unresolved' material. This homogenisation of the 'rest' material also requires a deter-

mination of its combined thermal conductivity in order to prescribe all thermal conductivities along with phase information to the heat conduction solver, described next in this section.

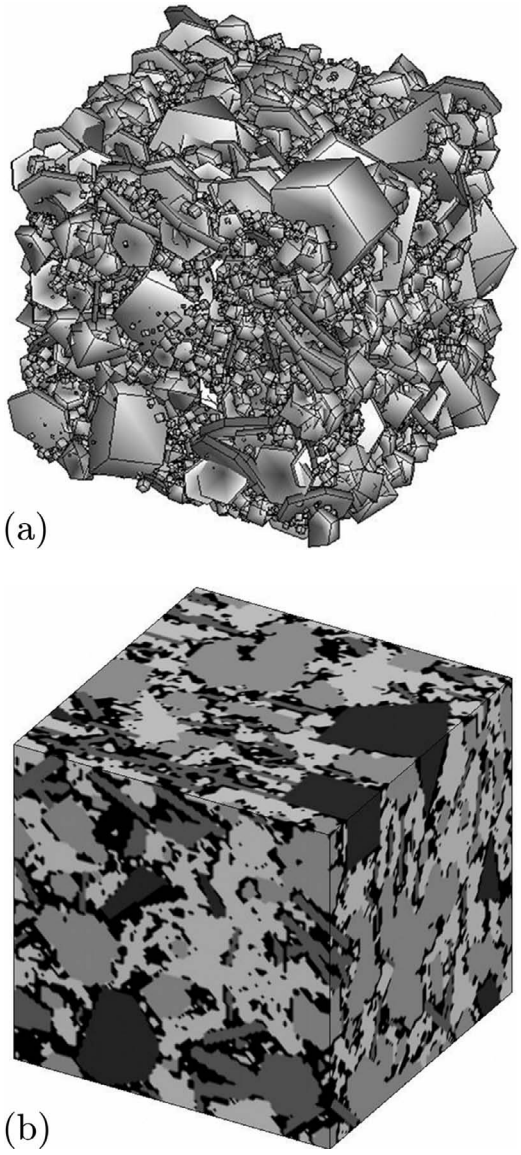

Fig. 1: Typical generated (a) refractory geometry along with its (b) discretisation on a uniform Cartesian grid.

(2) Thermal lattice-Boltzmann method

In this subsection, the TLBM using Single Relaxation Time (SRT), employed for some of the cases in the present investigation, is outlined. In TLBM, the macroscopic temperature T is represented by a microscopic distribution function g_i. The present problem requires the solution of heat conduction equation in the computation domain, generated using algorithms, described in the earlier subsection. In the SRT-TLBM, the energy equation is represented by the evolution equation of a corresponding distribution function g_i, which is known as the Lattice-Boltzmann Equation (LBE)

$$g_i(\boldsymbol{x}+\boldsymbol{e}_i\Delta t, t+\Delta t) = g_i(\boldsymbol{x},t) - \frac{1}{\tau_n}\left[g_i(\boldsymbol{x},t) - g_i^{\mathrm{eq}}(\boldsymbol{x},t)\right], \qquad (1)$$

where $\boldsymbol{x}$ is the position vector, t denotes the time, Δt represents the time step, $\boldsymbol{e}_i$ are the discrete lattice velocities, g_i^{eq} stands for the i^{th} component of the equilibrium distribution function and τ_n is the dimensionless relaxation time of the n^{th} phase. A three-dimensional (3-D) fifteen-speed D3Q15 stencil [13], which is schematically shown in Fig. 2, is used in the present investigation. The discrete lattice velocities for this stencil are given as: [13,38]

$$\boldsymbol{e}_i = \begin{cases} (0,0,0) & i=0 \\ (\pm 1,0,0)c,(0,\pm 1,0)c,(0,0,\pm 1)c & i=1,\ldots,6 \\ (\pm 1,\pm 1,\pm 1)c & i=7,\ldots,14 \end{cases} \qquad (2)$$

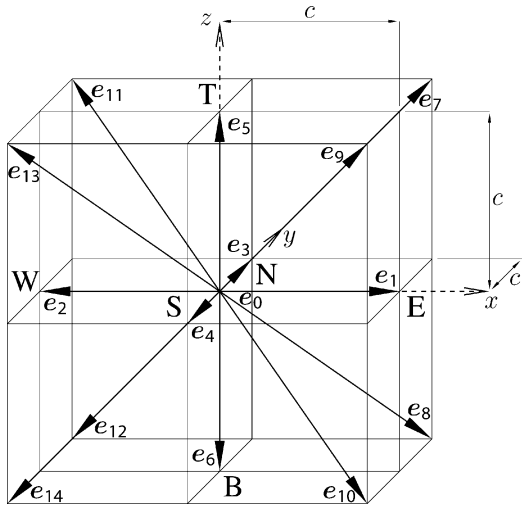

Fig. 2: Discrete velocities $\boldsymbol{e}_i$, given by Eq. (2), representing the D3Q15 stencil employed in the SRT-TLBM in a Cartesian frame of reference.

A macroscopic quantity, e.g. temperature T for the present problem, is given by the zeroth moment of the distribution function which reads:

$$T = M_0 = \sum_{i=0}^{14} g_i \qquad (3)$$

In order to express the equilibrium distribution function g_i^{eq} in the LBE (1), the weights, corresponding to the lattice velocities given by Eq. (2), are obtained as: [38]

$$w_i = \begin{cases} \frac{2}{9} & i=0 \\ \frac{1}{9} & i=1,\ldots,6 \\ \frac{1}{72} & i=7,\ldots,14 \end{cases} \qquad (4)$$

Employing these weights, the equilibrium distribution function is derived as: [13,39]

$$g_i^{\mathrm{eq}} = \begin{cases} 0 w_i M_0 = 0 & i=0 \\ 1 w_i M_0 = \frac{1}{9}T & i=1,\ldots,6 \\ 3 w_i M_0 = \frac{1}{24}T & i=7,\ldots,14 \end{cases} \qquad (5)$$

When the D3Q15 stencil, in conjunction with the equilibrium distribution function given by Eq. (5), is used in the SRT-TLBM, the dimensionless relaxation time for the n^{th} phase can be shown as: [13,39]

$$\tau_n = \frac{9}{5}\frac{a_n}{c^2\Delta t} + 0.5, \qquad (6)$$

where a_n is the thermal diffusivity of the n^{th} phase (component).

Without the loss of generality, a cubic domain is considered for the determination of k_{eff} of refractory materials. The heat conduction equation, represented by the LBE (1), is solved accounting for two isothermal cold and hot boundaries (surfaces) facing each other at temperatures T_c and T_h, where uniform Dirichlet boundary conditions are imposed. The remaining faces of the computational domain are considered adiabatic, i.e. homogeneous Neumann boundary condition with zero normal gradient is applied to them.

Once the steady-state solution of the LBE is obtained, k_{eff} of the modelled refractory material can be determined from the average steady-state heat flux $\dot{q}''_{\text{av}}$ based on the averaged Fourier's law of heat conduction according to

$$k_{\text{eff}} = \frac{L}{T_h - T_c}\dot{q}''_{\text{av}} = \frac{L}{T_h - T_c}\frac{\int_A \dot{q}''\,\mathrm{d}A}{\int_A \mathrm{d}A}, \tag{7}$$

where L is the distance across which the temperature difference is applied between the hot and cold walls and A is the cross-sectional area normal to the direction of average heat flow. In TLBM, the heat flux is determined from the distribution function g_i using the relation [13,40]

$$\dot{q}'' = \left(\sum_{i=0}^{14} \boldsymbol{e}_i g_i\right)\frac{\tau_n - 0.5}{\tau_n} \tag{8}$$

The presented TLBM has been implemented in an in-house computer code and verified against standard heat conduction problems [37], where a comparison with available analytical solutions has been drawn. Since the computational time, required for the solution of LBE for large, complex, multiphase domain, could be extremely high, the code has also been parallelised.

(3) Finite volume method

In order to carry out the sensitivity analysis to be presented in section IV, the FVM is also employed for solving the conduction heat transfer through the modelled refractory material. This grid-based method solves the integral form of the heat conduction equation

$$\int_V \varrho c_p \frac{\partial T}{\partial t}\mathrm{d}V = \int_V \nabla\cdot(k\nabla T)\mathrm{d}V, \tag{9}$$

where the solution domain is divided into a finite number of control volumes. However, the numerical grid, constructed in this manner, defines the edges of control volumes instead of the nodes, which is a common practice and nodes are placed at centres of each of these control volumes. In order to facilitate the application of boundary conditions, additional nodes are also arranged at boundary surfaces, edges and corners of the domain. The integral conservation equation (9) is valid for each control volume as well as for the entire domain. Thus, the physical conservation law is globally satisfied by the method. In the present study, the computational domain, representing the structure of refractory material, is subdivided by an equidistant Cartesian grid, similar to the one used for TLBM simulations.

The heat conduction equation is solved by performing the integration of Eq. (9) over the control volume of size $\Delta V = \Delta x\Delta y\Delta z$ by suitably expressing the time derivative on its left hand side over a time step size Δt. The spatial derivatives on the right hand side of Eq. (9) are discretised and expressed by a second-order accurate central differencing scheme. There exist different approaches for representing the right hand side in time, resulting in different numerical methods, e.g. explicit, Crank-Nicolson and fully implicit method. The result of this integration and the discretisation procedure is a linear equation for each control volume relating the temperature difference experienced throughout the time step at the corresponding node to temperatures at neighbouring nodes.

Once the heat conduction equation is solved by FVM, the effective thermal conductivity of the modelled geometry can be obtained from Eq. (7), as before. The heat fluxes appearing in Eq. (7) are, however, obtained directly from the known temperature gradients at the relevant boundary. The present in-house FVM code is also suitably parallelised in order to reduce the overall computational time for solution. In addition, both TLBM and FVM codes are validated by solving different benchmark problems involving heat conduction through solids, although these results are not presented here for the sake of brevity [37].

IV. Results and Discussion

Results presented in this section concern the sensitivity of effective thermal conductivity of the composite refractory material, numerically determined for room temperature conditions, towards different parameters used in the computational model. In this compilation, the influences of the direction of applied temperature gradient, the randomness of generated geometry and the modelled grain shapes as well as the effect of combined thermal conductivity of the 'rest' material on the effective thermal conductivity of the modelled refractory material are presented. The modified RSA algorithm is employed for the geometry generation in the following, unless otherwise stated.

The isotropy of generated random geometries with respect to the resulting thermal conductivity is first checked. In this study, the CDLM is employed in order to generate the random phase distribution and polyhedral grains are employed for the components. For one generated sample of each type of material considered, the effective thermal conductivity is determined from TLBM simulations accounting for the temperature gradient in each of the Cartesian coordinate directions. Results are presented in the first three columns of Table 3, from which, it can be identified that the direction of applied temperature gradient has only a minor influence on the effective thermal conductivity of modelled material and hence the generated structure for computational model can be considered nearly isotropic.

Table 3: Effective thermal conductivities of considered compositions in W/mK with respect to variations of grain shape and directions of applied temperature gradient.

Grain shape	Polyhedra			Spheres			Ellipsoids		
Material	Direction of ∇T			Direction of ∇T			Direction of ∇T		
	x	y	z	x	y	z	x	y	z
S10	36.94	37.02	37.36	36.80	36.85	36.79	37.76	36.63	36.72
AS	46.92	47.01	47.75	46.90	46.99	46.96	47.87	46.81	46.82
BT	49.25	49.37	49.98	49.30	49.34	49.29	50.09	49.13	49.13

Table 4: Effective thermal conductivities of considered compositions in W/mK with respect to different polyhedral grain shapes.

Tabular and fused alumina	Pentagonal prisms			Hexagonal prisms		
Coarse graphite (prisms)	Cuboid	Hexag.	Octag.	Cuboid	Hexag.	Octag.
S10 composition	35.84	36.11	36.01	35.99	36.11	36.00
AS composition	45.99	46.11	46.06	46.02	46.15	45.97
BT composition	48.52	48.40	48.41	48.26	48.46	48.56

The effect of randomly generated computational domain on the effective thermal conductivity is investigated next. For this purpose, ten different random geometries with the same volume fractions of constituents, representing the material S10, are generated. It is important to note here that the generated geometry is restricted by pre-assigned volume fractions, grain size distributions, grain shapes and rules of the geometry generation algorithm. Therefore, the phase distribution cannot be regarded completely random, but the generated geometry exhibits some kind of constrained random features. The effective thermal conductivity of each of the ten randomly generated geometries is determined from the solution of heat conduction equation, using TLBM. From these computations, the maximum and the minimum values of k_{eff} are obtained as 37.00 W/mK and 36.22 W/mK, respectively, with an average value of 36.64 W/mK and a standard deviation of only 0.29 W/mK. Since the magnitude of standard deviation is only about 0.8 % of the average value, the generated randomness in the geometry can be considered to have almost no effect on the determined k_{eff}.

In order to study the influence of grain shape on k_{eff} of the modelled refractory material, the CDLM is used for the generation of phase distributions in the computational domain. The values of k_{eff} obtained for three compositions comprising spherical and ellipsoidal grains are presented in Table 3. Since the deviations of values given in this table are of an order less than or equal to 2 %, it is evident that the shape of grains only has marginal influence on the determined values of k_{eff}.

In addition, the sensitivity of the determined k_{eff} towards the shape of polyhedral grains is also explored. For this study, the CDLM is employed for the geometry generation and the heat conduction equation is solved by the FVM. Tabular and fused alumina grains are modelled as either pentagonal or hexagonal prisms, while coarse graphite is represented by either cuboids or hexagonal or octagonal prisms. Effective thermal conductivities obtained from the FVM solutions for all the three materials and different shapes of polyhedral grains are presented in Table 4. From the values given in this table, it is obvious that the shape of polyhedral grains does not affect the determined k_{eff} to a great extent, as deviations below 1 % are only observed.

The fine-scaled material that could not be resolved by the computational model and is treated as a continuous phase consists of fine graphite, amorphous carbon and porosity as well as nanoscaled additives, as components, shown in Table 2. In the computational model, a thermal conductivity for this phase representing the 'rest' material is required. The combined thermal conductivity of 'rest' material is estimated based on the upper Hashin-Shtrikman [41] bound given by

$$k^{\text{HS,up}} = \frac{1}{\sum_n \frac{\phi_n}{2k_{\max} + k_n}} - 2k_{\max} \tag{10}$$

where n phases with volume fractions ϕ_n and thermal conductivities k_n are employed. Considering the lower limit for thermal conductivity of graphite as given in Table 2, the estimates of thermal conductivity of 'rest' material calculated employing the upper Hashin-Shtrikman bound given by Eq. (10), where ϕ_n are the modified volume fractions of constituents with respect to the 'rest' material, are 21.76 W/mK, 37.83 W/mK and 44.08 W/mK for S10, AS and BT material compositions, respectively. In order to study the sensitivity aspect, the conductivity of 'rest' material is assumed to be normally distributed with the mean μ, given by the aforementioned value corresponding to the upper Hashin-Shtrikman bound, and a standard deviation $\sigma = 0.1\mu$ (10 % of the mean). Ten equidistant values in the interval $[\mu - 3\sigma, \mu + 3\sigma]$ are then employed as the thermal conductivity of the 'rest' material for all three composi-

tions. The overall k_{eff} is evaluated from the results of FVM simulations and shown in Fig. 3. A linear regression analysis of the numerical data proves that effective thermal conductivities are linear functions of the combined thermal conductivity of the 'unresolved' material for each composition, as can be observed from this figure.

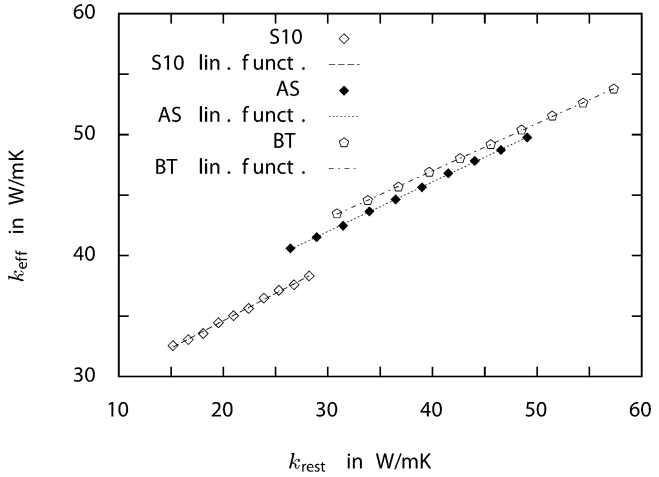

Fig. 3 : Effect of thermal conductivity of 'rest' material on k_{eff}.

Further in the present investigation, the influence of overlapping of grains is assessed for the BT material composition. Although several constraints on the allowed overlapping volume fraction ranging between 20 % and 100 % are tested, no significant difference in the resulting effective thermal conductivity is found. Hence the overlapping volume fractions of the grains have no major influence on the effective thermal conductivity. Another investigation, related to the effect of chosen geometry generation algorithm, is also carried out. Once again, no significant influence on the effective thermal conductivity is perceived.

V. Conclusions

In the present paper, a methodology for modelling the effective thermal conductivity of novel refractory materials with reduced carbon content is described. An analysis of sensitivity of k_{eff} towards different parameters of the computational model is also performed. From the latter, it is observed that k_{eff} is almost insensitive to the direction of applied temperature gradient, the randomly generated sample representing a particular composition and the chosen shape of grains in the numerical model. This indicates that the geometry generation algorithm produces truly random (obeying certain constraints), isotropic samples of refractory materials.

On the other hand, the effective thermal conductivity of modelled refractory is found to be a linear function of the combined thermal conductivity of the unresolved 'rest' material. Therefore, the focus of ongoing research work should be directed towards the reliable determination of k_{rest}. This can be done both experimentally by preparing only the 'rest' material itself and measuring its combined thermal conductivity as well as numerically based on a multiscale approach. The latter requires modelling the 'rest' material itself as a new composite, once again using a similar stochastic geometry generation algorithm, but on a substantially smaller scale, e.g. of 10 μm domain size. The resulting effective thermal conductivity of the 'rest' material, determined in a manner analogous to the one presented in this article, should then serve as an input parameter for the larger model (cube of side 2 mm, for example) discussed in this paper, and is expected to provide more reliable estimations.

Acknowledgement

The authors would like to gratefully acknowledge the financial support from the German Research Foundation (DFG) under the grants TR 470/2 – 1 and TR 470/2 – 2 in the framework of the priority programme SPP 1418 "Refractories-Initiative to Reduce Emissions" (FIRE).

References

1 Garbers-Craig, A.M.: How cool are refractory materials?, *J. South. Afr. Inst. Min. Metall.*, **108**, 491 – 506, (2008).

2 Tomeczek, J., Suwak, R.: Thermal conductivity of carbon-containing refractories, *Ceram. Int.*, **28**, 601 – 607, (2002).

3 Barea, R., Belmonte, M., Osendi, M.I., Miranzo, P.: Thermal conductivity of Al_2O_3/SiC platelet composites, *J. Eur. Ceram. Soc.*, **23**, 1773 – 1778, (2003).

4 Veyret, D., Cioulachtjian, S., Tadrist, L., Pantaloni, J.: Effective thermal conductivity of a composite material: a numerical approach, *J. Heat Transfer*, **115**, 866 – 871, (1993).

5 Zhou, H., Zhang, S., Yang, M.: The effect of heat-transfer passages on the effective thermal conductivity of high filler loading composite materials, *Compos. Sci. Technol.*, **67**, 1035 – 1040, (2007).

6 Maxwell, J.C.: A treatise on electricity and magnetism. Clarendon Press, Oxford, 1873.

7 Petrasch, J., Schrader, B., Wyss, P., Steinfeld, A.: Tomography-based determination of the effective thermal conductivity of fluid-saturated reticulate porous ceramics, *J. Heat Transfer*, **130**, 032602 (10 pp.), (2008).

8 Dondero, M., Cisilino, A.P., Carella, J.M., Tomba, J.P.: Effective thermal conductivity of functionally graded random micro-heterogeneous materials using representative volume element and BEM, *Int. J. Heat Mass Transfer*, **54**, 3874 – 3881, (2011).

9 He, X., Chen, S., Doolen, G.D.: A novel thermal model for the lattice Boltzmann method in incompressible limit, *J. Comput. Phys.*, **146**, 282 – 300, (1998).

10 Wang, M., Pan, N.: Predictions of effective physical properties of complex multiphase materials, *Mater. Sci. Eng., R*, **63**, 1 – 30, (2008).

11 Qian, J., Li, Q., Yu, K., Xuan, Y.: A novel method to determine effective thermal conductivity of porous materials, *Sci. China, Ser. E: Technol. Sci.*, **47**, 716 – 724, (2004).

12 Wang, M., Wang, J., Pan, N., Chen, S.: Mesoscopic predictions of the effective thermal conductivity for microscale random porous media, *Phys. Rev. E*, **75**, 036702 (10 pp.), (2007).

13 Wang, M., Wang, J., Pan, N., Chen, S., He, J.: Three-dimensional effect on the effective thermal conductivity of porous media, *J. Phys. D.: Appl. Phys.*, **40**, 260 – 265, (2007).

14 Wang, M., He, J., Yu, J., Pan, N.: Lattice Boltzmann modeling of the effective thermal conductivity for fibrous materials, *Int. J. Therm. Sci.*, **46**, 848 – 855, (2007).

15 Wang, M., Pan, N., Wang, J., Chen, S.: Mesoscopic simulations of phase distribution effects on the effective thermal conductivity of microgranular porous media, *J. Colloid Interface Sci.*, **311**, 562 – 570, (2007).

16 Wang, M., Meng, F., Pan, N.: Transport properties of functionally graded materials, *J. Appl. Phys.*, **102**, 033514 (7 pp.), (2007).

[17] Roungos, V., Aneziris, C.G., Berek, H.: Novel Al_2O_3-C refractories with less residual carbon due to nanoscaled additives for continuous steel casting applications, *Adv. Eng. Mater.*, **14**, 255 – 264, (2012).

[18] Roungos, V., Aneziris, C.G.: Improved thermal shock performance of Al_2O_3-C refractories due to nanoscaled additives, *Ceram. Int.*, **38**, 919 – 927, (2012).

[19] Brachhold, N., Aneziris, C.G., Stein, V., Roungos, V., Moritz, K.: Low carbon content and carbon-free refractory materials with high thermal shock resistance, (in German), *Keram. Z.*, **64**, 109 – 114, (2012).

[20] Stein, V.: Contribution to the characteristic improvement of carbon bonded doloma refractories by addition of functional ceramic materials, Ph.D. thesis, Technische Universität Bergakademie Freiberg, Freiberger Forschungshefte, A 905, (2011).

[21] Schwieger, K.-H.: Feuerfestmassen. In: Becker, G.W., Braun, D., Woebcken, W. (Eds.): Kunststoffhandbuch, Vol. 10 Duroplaste, (in German), Carl Hanser Verlag, München, 1096 – 1104, 1988.

[22] Irie, S., Rappolt, J.: Phenolic resin for refractories. In: Pilato, L.: Phenolic Resins: A Century of Progress, Springer-Verlag, Berlin, chapter 19, 503 – 515, 2010.

[23] Haynes, W.M., Lide, D.R., Bruno, T.J. (Eds.): CRC Handbook of Chemistry and Physics. 94th edition. CRC Press, Boca Raton, 2013.

[24] Klein, C., Hurlbut, Jr., C.S.: Manual of Mineralogy. 21st edition. John Wiley & Sons, New York, 1999.

[25] Martin, C.A., Sandler, J.K.W., Shaffer, M.S.P., Schwarz, M.-K., Bauhofer, W., Schulte, K., Windle, A.H.: Formation of percolating networks in multi-wall carbon-nanotube-epoxy composites, *Compos. Sci. Technol.*, **64**, 2309 – 2316, (2004).

[26] Slobodian, P., Riha, P., Lengalova, A., Svoboda, P., Saha, P.: Multi-wall carbon nanotube networks as potential resistive gas sensors for organic vapor detection, *Carbon*, **49**, 2499 – 2507, (2011).

[27] Anthony, J.W., Bideaux, R.A., Bladh, K.W., Nichols, M.C.: Handbook of mineralogy - Vol. III: Halides, Hydroxides, Oxides. Mineral Data Publishing, Tucson, 1997.

[28] Thostenson, E.T., Chou, T.-W.: On the elastic properties of carbon nanotube-based composites: modelling and characterization, *J. Phys. D: Appl. Phys.*, **36**, 573 – 582, (2003).

[29] Granqvist, C.G., Buhrmann, R.A.: Ultrafine metal particles, *J. Appl. Phys.*, **47**, 2200 – 2219, (1976).

[30] Kiss, L.B., Söderlund, J., Niklasson, G.A., Granqvist, C.G.: New approach to the origin of lognormal size distributions of nanoparticles, *Nanotechnology*, **10**, 25 – 28, (1999).

[31] Matheron, G.: Random sets and integral geometry. John Wiley & Sons, New York, 1975.

[32] Feder, J.: Random sequential adsorption, *J. Theor. Biol.*, **87**, 237 – 254, (1980).

[33] Torquato, S.: Random heterogeneous materials: microstructure and macroscopic properties. Springer-Verlag, New York, 2002.

[34] Ballani, F., Daley, D.J., Stoyan, D.: Modelling the microstructure of concrete with spherical grains, *Comput. Mater. Sci.*, **35**, 399 – 407, (2006).

[35] Goldstein, H., Poole, C.P., Safko, J.L.: Classical mechanics. Third edition, Addison-Wesley, San Francisco, 2002.

[36] ISO 1151 – 1, Flight dynamics - Concepts, quantities and symbols – Part 1: Aircraft motion relative to the air, 1988.

[37] Zehmisch, R., Al-Zoubi, A., Ray, S., Trimis, D., Ballani, F., van den Boogaart, K.G.: Numerical determination of effective thermal conductivity of refractory materials, *Refractories Worldforum*, **4**, 181 – 186, (2012).

[38] Qian, Y.H., d'Humières, D., Lallemand, P.: Lattice BGK models for Navier-Stokes equation, *Europhys. Lett.*, **17**, 479 – 484, (1992).

[39] Peng, Y., Shu, C., Chew, Y.T.: A 3D incompressible thermal lattice Boltzmann model and its application to simulate natural convection in a cubic cavity, *J. Comput. Phys.*, **193**, 260 – 274, (2004).

[40] D'Orazio, A., Succi, S.: Boundary conditions for thermal lattice Boltzmann simulations. In: Sloot, P.M.A., Abramson, D., Bogdanov, A.V., Dongarra, J.J., Zomaya, A.Y., Gorbachev, Y.E. (Eds.): Computational Science — ICCS 2003, Lecture Notes in Computer Science, **2657**, Springer-Verlag, Berlin, 977 – 986, 2003.

[41] Hashin, Z., Shtrikman, S.: A variational approach to the theory of the effective magnetic permeability of multiphase materials, *J. Appl. Phys.*, **33**, 3125 – 3131, (1962).